Thermodynamic Simulation of Rocket Nosecones During Ascent

Eric Souder

July 2022

Abstract

Method of modeling the heating of rocket vehicle nosecones, and application of the model in simulating the temperature change in UBC Rocket's Whistler-Blackcomb flight to 100 km. The simulation results show that the nosecone rapidly heats to 540K and plateaus at this temperature. It is concluded that care must be taken in the design of the vehicle to choose nosecone materials that can withstand this heat and to appropriately insulate sensitive electronics in the nosecone to ensure they function over the entire flight.

1 Introduction

During the launch of a sounding rocket into sub-orbital flight, the exterior of the vehicle experiences heat loading, concentrated towards the angled nosecone face of the rocket that directly encounters the air stream as it accelerates upward. Insight into the specifics of this heating is critical in the design process to ensure that a rocket vehicle is constructed out of materials that will not fail and in a manner that maintains internal temperatures at appropriate levels for components housed inside the nosecone. This knowledge is critical not only to the success of the mission, but also the safety of observers and operators in the vicinity of the spacecraft. For this reason, modeling of the nosecone has been investigated by many authors over many years. This paper incorporates results and ideas from previous works to present a simple model of nosecone heating for a sub-orbital rocket and a simulation, using this model, of an ascent of UBC Rocket's Whistler-Blackcomb vehicle to roughly 100 kilometers.

2 Modeling Nosecone Skin Heating

Objects traveling at high speeds are subject to heating and cooling as they travel through the atmosphere. As a rocket vehicle travels at supersonic velocities, there are two significant contributions to the temperature change of the nosecone - the aerodynamic heating from the compression of air as the nosecone pushes through it, and the heat lost to the atmosphere through radiation. For the purposes of this analysis, these will be the only sources of thermal energy change considered.

2.1 Nosecone Aerodynamic Heating

As the nosecone travels at supersonic speeds, it forms a shock wave as it moves faster than the air can escape. From the frame of reference of the vehicle, This can be considered as air being blown towards a stationary nosecone, at the speed the rocket would be traveling. At the very tip of the nosecone, the air has zero relative velocity to the vehicle. This is the stagnation point. [6]

At the stagnation point, all the kinetic energy of the air is converted into thermal energy. Because this process happens so quickly, it can be modeled as an adiabatic compression of gas.

$$PV^{\gamma} = \text{constant}$$

The ideal gas approximation ($V \propto TP^{-1}$) can be applied, so

$$P^{1-\gamma}T^{\gamma} = \text{constant}$$

In our compression, this means

$$\frac{T_s}{T_0} = \left(\frac{P_s}{P_0}\right)^{\frac{\gamma-1}{\gamma}}$$

With T_s, P_s as the stagnation temperature and pressure and T_0, P_0 as the static temperature and pressure. The relation between the static and stagnation pressure of a gas is sourced from a National Advisory Committee for Aeronautics report on compressible flow [8]:

$$\frac{P_s}{P_0} = \left(1 + \frac{\gamma-1}{2}M^2\right)^{\frac{\gamma}{\gamma-1}}$$

Where M is the mach number. This provides an equation for stagnation temperature as a function of speed:

$$\frac{T_s}{T_0} = 1 + \frac{\gamma-1}{2}M^2$$

Of course, the entire nose cone will not encounter air at the stagnation temperature. Most air will be slowed, but stopped by skin friction with the vehicle, forming a boundary later around the nosecone. Toft models the average temperature of this boundary layer air (T_B) based on K, a temperature recovery factor [9]:

$$K = \frac{T_B - T_0}{T_s - T_0}$$

Eber provides a value of $K = 0.89$ for cones with vertex angles between 20 and 50 degrees [2].

We then have an equation for the temperature of the boundary layer:

$$T_B = KT_s + T_0\,(1 - K)$$

Eber also provides an experimentally modeled value for h, the heat transfer function[1] [2]:

$$h = \left(0.0071 + 0.0154\sqrt[2]{\beta}\right)\frac{k}{\mu^{0.8}l^{0.2}}\,(\rho_0 u)$$

[1]Note that this equation is accurate only for values of μ, k, l, etc. in the US customary system. When determining this value for use in simulations, care should be taken to mind unit conversions.

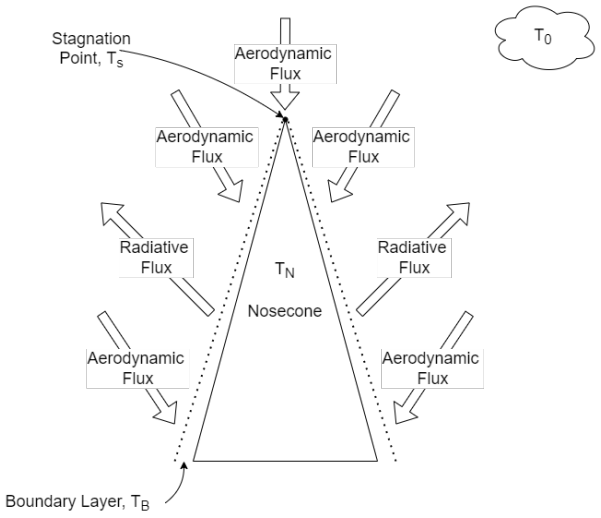

Figure 1: Thermal fluxes acting on the nosecone

Based on k, the thermal conductivity of air; β, the vertex angle of the cone; ρ, the density of the air; μ, the dynamic viscosity of air; u the velocity of the rocket; and l, the length of the cone measured along the surface.

With all this, we can determine the heat flux into the nosecone skin from aerodynamic effects:

$$\dot{Q}_{aero} = h(T_B - T_N)$$

Where T_N is the actual temperature of the nosecone skin.

2.2 Radiative Effects

Some amount of heat flux leaves the nosecone as blackbody radiation, with heat flux $\dot{Q}_r ad = \epsilon\sigma(T_0^4 - T_N^4)$, where ϵ is the emissivity of stainless steel and σ is the Stefan-Boltzmann constant.

This situation as well as the effects of section 2.1 above is generalized in figure 1, showing the fluxes into and out of the nosecone as well as the locations of the various temperatures used in the calculation. Note that the direction of the flux arrows is generalized, and they may point in opposite directions at different points during the flight.

2.3 Flight Profile

In order to model the thermal behavior of the nosecone, we must provide a number of inputs to our aerodynamic heating simulation functions based on altitude and velocity. These inputs are provided by UBC Rocket's proprietary Feynman vehicle design program.

Although Feynman was originally intended for optimizing the design of rocket vehicle components, such as fins, engines, or nosecones for maximum altitude without regard for thermal effects, its outputs are helpful in the analysis of the nosecones thermal properties.

Feynman provides data for Mach number and altitude at 10 millisecond intervals for the first approximately 160 seconds of flight, corresponding to a peak altitude of almost 100 kilometers and a maximum speed of more than mach 4. For this reason, we can use the output data of the Feynman simulation as a reasonable input flight profile for our thermal analysis.

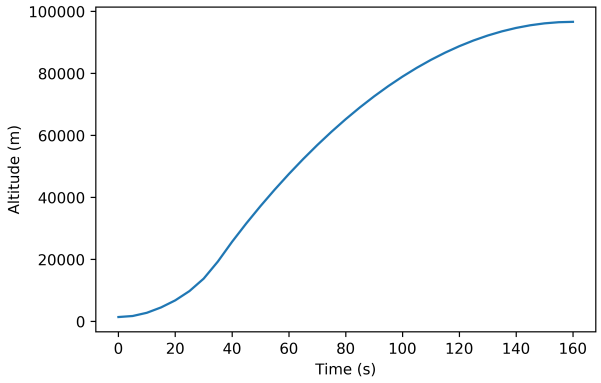

Figure 2a: Altitude over Time of simulated vehicle trajectory

Additionally, empirically-derived curves for ρ_0 and T_0 in terms of altitude and of μ and k in terms of T_0 are provided in appendix A. These provide a full picture of the conditions around the nosecone over all stages of the flight.

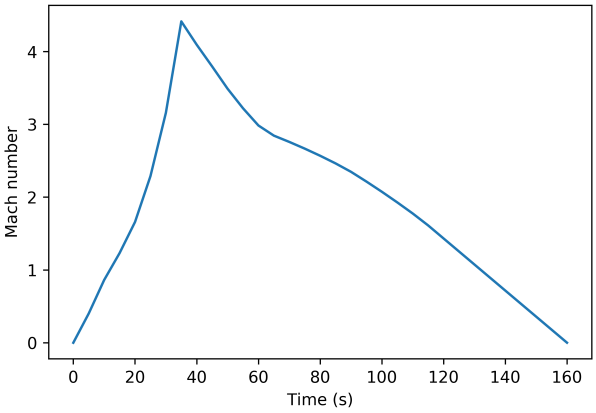

Figure 2b: Mach number over time of simulated vehicle trajectory

2.4 Heat Flux Balance

Expanding on the first law of thermodynamics, our simulation must respect the conservation of energy. Thus, the nosecone situation through flight can be modeled by an energy balance:

$$\text{Heat Flux In} = \text{Heat Flux out}$$

This can be modeled by the heat equation:

$$GdT_N = dt(\dot{Q}_{aero} - \dot{Q}_{rad})$$

or

$$dT_N = \frac{dt(\dot{Q}_{aero} - \dot{Q}_{rad})}{G} \tag{1}$$

With a factor G, the 'skin heating capacity' [5] determined by the specific heat of the nosecone skin c, it's thickness τ, and it's density ρ.

$$G = c\tau\rho$$

2.5 Simulation Method

Considering a small but finite change in time Δt (in our simulation case, $10ms$, from Feynman as above), we can numerically solve for the change ΔT_N in the nosecone temperature based on equation 1 above.

This solution is determined by means of a python simulation which iterates over each timestep and calculates the change in T_N for that time. Using the atmospheric models from appendix A and the constant values from appendix B, a representative model of the at-rest (i.e. far away from the vehicle's path of flight) is created. Then, using the Feynman-derived data for Mach number and altitude, and the derived equations from the above sections, values are determined for $u, \mu, k, h, T_s, T_B, \dot{Q}_{aero}$ and $\dot{Q}_{rad}$, which are then used to solve for ΔT_N for the timestep, which then modifies T_N for use in the simulation of the next timestep.

3 Discussion of Results

3.1 General Discussion

Based on the above simulation, the temperature of the nosecone can be determined as a function of time as seen in figure 3 below. The peak temperature of 540 K occurs about 65 seconds into the flight. It is interesting to note that after the rapid rise in temperature, the decline after the peak is significantly shallower, nearly plateauing.

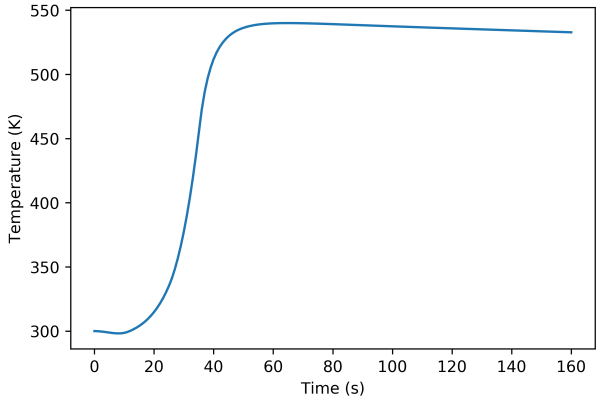

Figure 3: Temperature of nosecone skin over time

This is reasonable considering figure 4: the vast majority of the total heat flux at the skin of the rocket is due to aerodynamic effects, with the peak of the aerodynamic flux occurring generally at the same time as the peak mach number. This would seem to be a reasonable result. Considering the fixed-vehicle frame of reference, as air particles encounter the tip of the nosecone at higher speeds, they will have more kinetic energy, all of which will be transferred to the nosecone, increasing the kinetic energy of its constituent particles and so increasing its temperature more than at slower velocities. Since we expect the heating of the nosecone to be positively related to the stagnation temperature, we can expect higher aerodynamic fluxes at higher speeds.

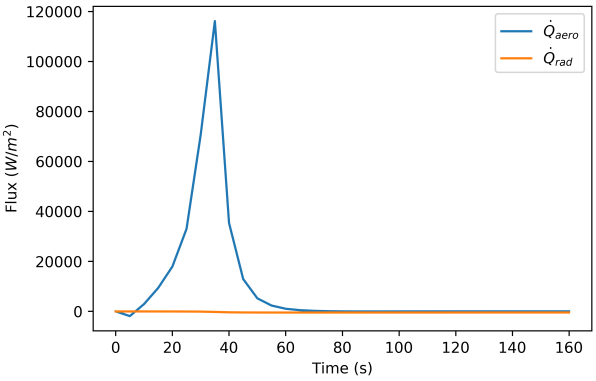

Figure 4a: $\dot{Q}_{aero}$ and $\dot{Q}_{rad}$ fluxes over time

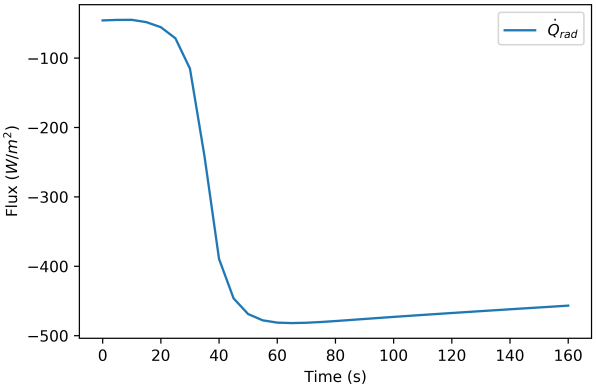

Figure 4b: Detail of $\dot{Q}_{rad}$ flux over time

The radiative effects, while not zero, are significantly smaller than the aerodynamic effects since the nosecone, while experiencing a large aerodynamic

flux, is not heated by a huge degree and so does not reach high enough temperatures to have the blackbody radiation play a large role in the total flux. Additionally, radiative effects are minimized by the low emissivity of the aluminum nosecone - about 0.1 - as it is quite far from a perfect blackbody. Further, the relatively low contribution of the radiative component to the overall simulation output validates our use of a constant ϵ in calculating emissivity over the entire flight, even though ϵ does vary with temperature.

Through Wien's displacement law, $\lambda_{\text{peak}} = \frac{b}{T_N}$, we can predict the peak wavelength of the nosecone's emitted radiation, as shown in figure 5.

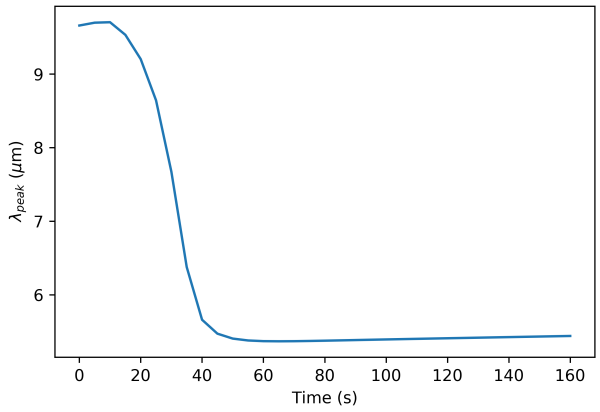

Figure 5: Peak wavelength λ_{peak} emitted by the nosecone over time

Since this curve falls strictly within the infrared range, 780 nm to 1 mm, there will be no visible indication of the temperature of the nosecone.

We can also predict the temperature of air at the stagnation point and boundary layer, seen in figure 6.

Although the peak stagnation temperature and boundary layer temperatures are quite high, both over 1000K (1139K and 1039K, respectively), we do not observe these temperatures in the nosecone skin. Partially, this can be understood from the observation that the peak temperatures occur only briefly, shooting up rapidly and cooling to lower temperatures relatively fast. As well, the aluminum has

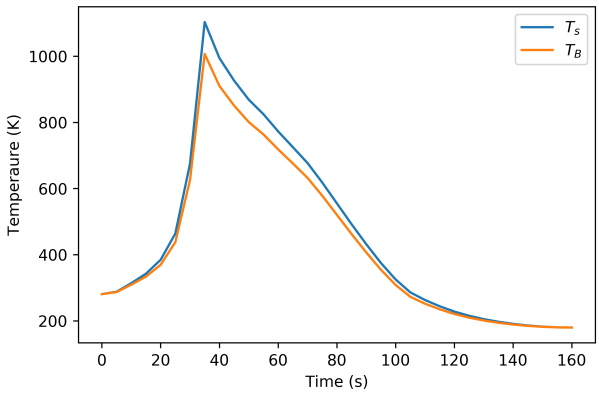

Figure 6: Stagnation point and boundary layer temperatures over time

a skin-heating capacity G greater than one, so the change in its temperature is moderated by G in addition to the amount of flux it receives.

3.2 Implications for Avionics Hardware Housed in Nosecone

Onboard the Whistler-Blackcomb rocket, many of the avionics components are housed within the nosecone, including the main flight computer, which is responsible for directing most of the primary guidance, navigation, safety, and recovery functions of the avionics system during the flight. For this reason, it is necessary that it functions throughout the entire flight. The NXP MK66FX microcontroller chip used in the main flight computer has a maximum ambient temperature rating of 105 degrees Celsius [7], or 378.15K. As this is below the peak temperature of the nosecone skin, some care and analysis will be necessary in determining the placement of the flight computer so that it does not reach the same temperature as the nosecone.

Assuming that the heat capacity of the flight computer is insignificant compared to that of the nosecone - a reasonable assumption since the mass of the flight computer is minimal ($\frac{m_{\text{computer}}}{m_{\text{nosecone}}} \approx 0$) - then we know it would be unwise to mount the flight computer directly to the interior skin of the nosecone.

Considerations will have to be made in the placement of avionics, such as thermally insulating it from the metal of the nosecone in order to ensure it continues to function over the duration of the flight.

If this were a steady state solution, the computer would eventually equilibrate to the temperature of the nosecone and fail. However, this plateau is not permanent - it will only last as long as the vehicle remains above an altitude where the h, the heat transfer coefficient is low and at speeds where atmospheric heating is a factor. At slow speeds with denser atmosphere, the aerodynamic flux reverses direction and moves energy from the high-temperature nosecone into the lower-temperature air.

Since we know the flight plan includes a long, slow descent from the upper atmosphere under ballutes and parachutes, design considerations do not need to be made to isolate the flight computer from the nosecone plateau temperature for an arbitrarily long amount of time, but for a finite time (measured in minutes) until the nosecone can be sufficiently cooled during reentry. However, more Feynman simulations at longer time intervals are needed to accurately determine this time.

4 Conclusions

The thermodynamic behavior of the UBC Rocket Whistler-Blackcomb vehicle's nosecone during launch was determined by means of a numerical simulation. The analysis showed that under a predicted flight profile reaching about 100 km in height at a maximum mach number of about 4, the average temperature of the nosecone skin reaches 540 K, an increase of 240 C from its initial temperature before launch. Based on this analysis, The analysis shows also that the heat increases rapidly during launch and then plateaus, presenting a concern for temperature-sensitive components housed inside the nosecone.

Additionally, this paper provides a generalized system of equations that can be used to solve by simulation the nosecone temperatures of a nosecone under various flight profiles. The provided system can only be used with nosecone shapes that fit within Eber's experimental range of nosecone angles, from 20 degrees to 50 degrees. This system also disregards sources of thermal flux outside atmospheric interactions and thermal radiation from the atmosphere; it does not consider flux sources such as the radiation output of the sun, the combustion in the engines of the vehicle, and the thermal sink of cryogenic fuels that may also be found on the vehicle. Finally, the system only provides information for the average representative temperature of the nosecone, which while suitable for further calculations inside the nosecone or with respect to the rest of the rocket, are not suitable for analyzing the performance of specific locations on the nosecone.

Appendices

A Atmospheric Models

A.1 Air Pressure as a function of Altitude

Air pressure P_0 as a function of altitude s, from [9] and [1].

$$P_0(s) = \begin{cases} \exp\left(4.43165 \cdot 10^{-14}s^3 - 2.28553 \cdot 10^{-9}s^2 - 1.14097 \cdot 10^{-4}s + 6.95109\right) & 0\text{km} < s \leq 25\text{km} \\ \exp\left(-2.28179 \cdot 10^{-14}s^3 + 3.34063 \cdot 10^{-}9s^2 - 2.84655 \cdot 10^{-4}s + 8.73033\right) & 25\text{km} < s \leq 75\text{km} \\ \exp\left(4.44813 \cdot 10^{-14}s^3 - 1.13434 \cdot 10^{-}9s^2 + 7.62651 \cdot 10^{-4}s - 15.5981\right) & 75\text{km} < s \leq 120\text{km} \end{cases}$$

A.2 Air Density as a function of Altitude

Air pressure ρ_0 as a function of altidue s, , from [9] and [1].

$$\rho_0(s) = \begin{cases} \exp\left(4.88158 \cdot 10^{-18}s^4 - 1.808 \cdot 10^{-13}s^3 + 2.432 \cdot 10^{-11}s^2 - 9.693 \cdot 10^{-5}s + 0.1922\right) & 0\text{km} < s \leq 25\text{km} \\ \exp\left(-6.034 \cdot 10^{-19}s^4 - 1.035 \cdot 10^{-13}s^3 - 5.746 \cdot 10^{-9}s^2 - 2.21 \cdot 10^{-5} - 0.396\right) & 25\text{km} < s \leq 75\text{km} \\ \exp\left(-1.004 \cdot 10^{-18}s^4 + 4.440 \cdot 10^{-13}s^3 - 7.137 \cdot 10^{-8}s^2 + 4.773 \cdot 10^{-5} - 121.84\right) & 75\text{km} < s \leq 120\text{km} \end{cases}$$

A.3 Air Temperature as a function of Altitude

Air Temperature, T_0, as a function of altitude s, from [9] and [1].

$$T_0(s) = \begin{cases} 287.954 - 5.03015 \cdot 10^{-3}s - 1.2859 \cdot 10^{-7}s^2 & 0\text{km} < s \leq 10\text{km} \\ 225.15 & 10\text{km} < s \leq 23\text{km} \\ 242.057 - 2.33854 \cdot 10^{-3}s + 7.08133 \cdot 10^{-8}s^2 & 23\text{km} < s \leq 42\text{km} \\ -534.104 + 3.95468 \cdot 10^{-2}s - 6.0177 \cdot 10^{-7}s^2 + 2.71838 \cdot 10^{-12}s^3 & 42\text{km} < s \leq 81.5\text{km} \\ 867.12 - 9.78603 \cdot 10^{-3}s - 5.75164 \cdot 10^{-8}s^2 + 8.81316 \cdot 10^{-13}s^3 & 81.5\text{km} < s \leq 120\text{km} \end{cases}$$

A.4 Dynamic Viscocity of Air as a function of Temperature

Dynamic Viscocity of Air, μ, as a function of Temperature T_0, from [9].

$$\mu(T_0) = -1.00 \cdot 10^{-5} - 1.47 \cdot 10^{-9}T + 1.68 \cdot 10^{-6}T^{\frac{1}{2}}$$

A.5 Thermal Conductivity of Air as a function of Temperature

Thermal Conductivity of Air, k, as a function of Temperature T_0, from [9].

$$k(T_0) = -1.29 \cdot 10^{-2} + 2.43 \cdot 10^{-5}T - 3.39 \cdot 10^{-9}T^2 + 1.88 \cdot 10^{-3}T^{\frac{1}{2}}$$

B Simulation Constants

Nosecone characteristic length: $l = 1m$
Nosecone vertex angle: $\beta = 30°$
Aluminum (6082 alloy) properties:
  Emissivity [4]: $\epsilon = 0.1$
  Specific heat capacity [3]: $c = 896 J/kg \cdot K$
  Skin thickness: $\tau = 0.0025m$
  Density [3]: $\rho = 2700 kg/m^3$

References

[1] National Aeronautics and Space Administration. U.s. standard atmosphere supplements, 1966. 60deg N, July.

[2] G. R. Eber. Experimentelle untersuchung der bremstemperatur und des wärmeüberganges an einfachen körpern bei Überschallgeschwindikeit. Technical report, Peenemünde Army Research Center, German Army Weapons Office, November 1941.

[3] Gleich Aluminium. *EN AW 6082 Technical Data Sheet*.

[4] Zorana Lanc, Branko Strbac, Milan Zeljkovic, Aleksandar Zivkovic, and Miodrag Hadzistevic. Emissivity of aluminium alloy using infrared thermography technique. *Materials and technology*, 3(52), 2018.

[5] Hsu Lo. Determination of transient skin temperature of conical bodies during short-time, high-speed flight. Technical report, Langley Aeronautical Laboratory, National Advisory Committee For Aeronautics, October 1948.

[6] NASA Glenn Research Center. *Stagnation Temperature Real Gas Effects*, May 2021.

[7] NXP Semiconductors. *Kinetis K66 Sub-Family 180 MHz ARM® Cortex®-M4F Microcontroller*, April 2017.

[8] Ames Research Staff. Equations and charts for compressible flow. Technical report, Ames Aeronautical Laboratory, National Advisory Committee For Aeronautics, 1953.

[9] Hans Olaf Toft. Simplified aerodynamic heating of rockets. Technical report, Dansk Amatør Raket Klub, August 2014.

License and Open-Source Information